IEEE Transactions on Power Electronics, pp. 1–15, 2022

Performance Analysis of Energy Balancing Methods for Matrix Modular Multilevel Converters

P. Bontemps, S. Milovanovic, and D. Dujic

POWER ELECTRONICS LABORATORY
ÉCOLE POLYTECHNIQUE FÉDÉRALE DE LAUSANNE

This article has been accepted for publication in IEEE Transactions on Power Electronics. This is the author's version which has not been fully edited and content may change prior to final publication. Citation information: DOI 10.1109/TPEL.2022.3215734

Performance Analysis of Energy Balancing Methods for Matrix Modular Multilevel Converters

Philippe Bontemps, *Student Member, IEEE,* Stefan Milovanovic, *Member, IEEE,* and Drazen Dujic, *Senior Member, IEEE*

***Abstract*—Modular multilevel converters achieve voltage scalability through the series connection of cells, each with its own capacitance. However, this converter structure using floating energy storage elements increases the control complexity significantly. The voltages of each capacitance must be controlled to their respective setpoints to ensure correct operation of the converter. Relying on the use of circulating currents, which are unobservable at the converter terminals, the energy can be exchanged among the branches. Three control principles resulting in three different implementations are thoroughly explained and their dynamic performance is compared. The results are verified using a hardware-in-the-loop platform simulating a hydro power plant using matrix modular multilevel converter connected between a 6.6 kV grid and a 6 kV synchronous machine.**

***Index Terms*—Hardware-in-the-Loop, Real-Time Simulations, Matrix Modular Multilevel Converter, Pumped Hydro Storage Power Plants, Variable Speed Drive**

I. Introduction

APPLICATIONS such as Pumped Hydro Storage Power Plants (PHSPs) with power levels exceeding 100 MW exclude the use of conventional multilevel converters [1]–[5]. However, such voltage and power ratings can be achieved by the Modular Multilevel Converter (MMC) topology due to its modularity [6], [7]. A theoretically unlimited voltage scalability results from the series connection of cells, each with their own capacitance. The floating nature of the cell capacitances requires special control algorithms to maintain a balanced cell voltage among all cells. Within the family of the MMC two topologies, namely the Matrix Modular Multilevel Converter (M3C) and the MMC can be distinguished and the former one is shown in Fig. 1. Due to its improved performance for variable speed drive applications, the M3C is the preferred option for PHSP applications and will be the focus of this paper [8]. Henceforth, it is assumed that the M3C is connected to a 3 phase ac grid on one side and a Synchronous Machine (SM) on the other one as illustrated in Fig. 1.

Maintaining a balanced voltage among all cells of the M3C introduces control challenges. A branch energy variation from its nominal value affects the cell voltages of the given branch, thus energy balancing among the cells is requires to ensure proper and safe operation of the M3C. An excessively high branch energy leads to premature aging or damaging of the components installed on the cell due to the higher cell capacitance voltage.

Three main categories of energy control can be distinguished in the M3C, namely the total energy control, the energy balancing among the branches and the energy balancing among the cells constituting the branch. A proper operation of the M3C is only possible with all the previously mentioned energy control layers working properly. The first category, the total energy control, ensures that the overall energy within the converter follows a given reference. During normal operation, the total energy balancing within the converter is achieved by ensuring that the input power is equal to the sum of the internal converter losses and the output power reference.

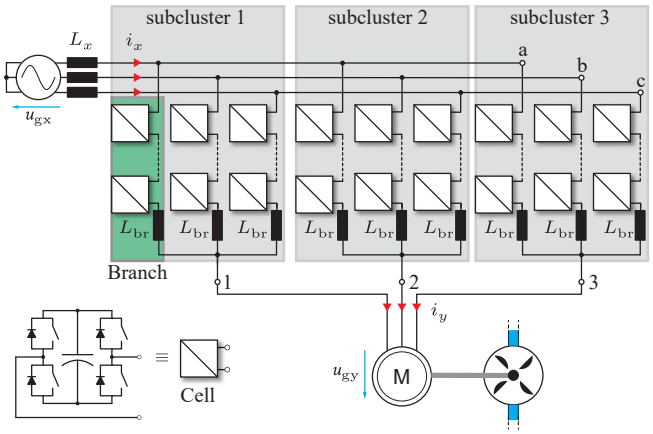

Fig. 1. The M3C with the three subclusters, highlighted in gray, each containing three branches, highlighted in green, and N cells per branch. The two AC systems connected to the terminals are represented by a grid on the input side and a 3 phase machine on the output side connected to a pump/turbine as is the case is a PHSP.

With a properly working total energy control, the energy present within the converter capacitances must be equally distributed among the nine branches. This leads to the necessity of an energy balancing method to allow the exchange of energy among the branches of the converter. To avoid altering the behavior of the converter and the total energy controller, these generated balancing currents should not influence the terminal currents of the converter. Circulating currents, which as the name suggests should remain circulating within the converter thus fulfilling the previously mentioned condition, are used for the purpose of energy balancing of the branches.

With the two energy control layers described above working fine, the last balancing action includes balancing of the energy within the cells belonging to the same branch. This balancing action is highly dependent on the applied modulation scheme, which in the case of this paper is the Phase Shifted Carrier (PSC) Pulse-Width Modulation (PWM) [9]–[11]. As the energy control among the cells of the branch will not be

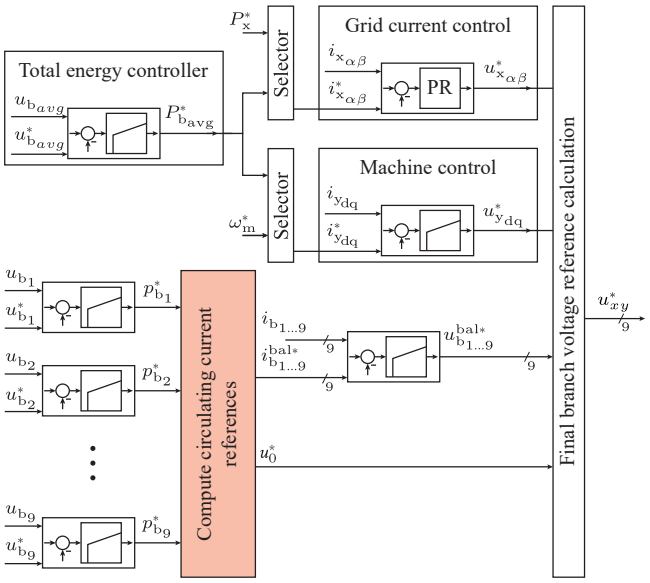

Fig. 2. Overview of the M3C control structure with the circulating current reference modification block, being the main focus of this paper, highlighted.

covered in this paper, no further consideration is given to the modulation scheme.

Fig. 2 shows the overall control structure of the M3C as implemented in this paper. The total energy control defines the power reference for either the grid current control or the machine control, depending on the operation mode of the PHSP. The internal energy balancing part is shown on the bottom of Fig. 2, with the reference modification block, being the focus of this paper, highlighted.

A report of the main energy balancing methods as well as a performance analysis for the MMC topology can be found in [12]. However, due to its topology, the M3C requires a different branch energy balancing control approach. Within the literature, three significantly different methods exist [13]–[18], which will be the scope of this paper. While achieving the same goal, these three approaches rely on different control principles. They are derived in different reference frames and trade offs in dynamic performance, ease of implementation and flexibility are not evident at first glance. Additionally, one of the presented methods [17] is not widely discussed in the literature and one can claim that a slight theoretical gap still exists in the theory of the M3C. This paper fills this gap by firstly explaining the basic operating principles of the three methods and subsequently bringing them into the same reference frame to allow for a thorough comparison in terms of operating performance and flexibility. Thereafter, possibility of deriving one method from the other is discussed, which makes the comparison conducted herewith comprehensive and valuable for control engineers dealing with the M3C.

The validation of the analytical findings is done by implementing the three methods on a Hardware-In-The-Loop (HIL) platform introduced in [19]. The results obtained from the HIL are of high fidelity given the usage of industrial controllers with real measurement and processing delays.

This paper is organized as follows, section II covers the basic operating principles of the M3C. Additionally, the requirements of the energy balancing algorithms and the assumptions made in this paper are elaborated. Section III includes a mathematical development of the three energy balancing algorithms compared in this work and section VI compares all the methods and illustrates their differences. Section V shows the results obtained on the RT-HIL platform and section VI concludes the work.

II. M3C OPERATING PRINCIPLES AND DEFINITIONS

The naming convention adopted throughout this paper is the following:

Input ac system:	$i_{\mathrm{x}}(t), u_{\mathrm{x}}(t)$	where	$\mathrm{x} \in [\mathrm{a,b,c}]$
Output ac system:	$i_{\mathrm{y}}(t), u_{\mathrm{y}}(t)$	where	$\mathrm{y} \in [1,2,3]$
M3C branches:	$i_{\mathrm{xy}}(t), u_{\mathrm{xy}}(t)$	where	$\mathrm{xy} \in [\mathrm{a1}, \ldots, \mathrm{c3}]$

Fig. 3 defines the current and voltage directions used in this paper. Based on these, the following branch equations can be developed as (1) and (2). The branch currents expression as seen in (2) has in addition to the input and output terminal currents a third component which is the previously mentioned circulating currents. While the branch voltage expression also contains the component driving the circulating current, this voltage component is negligible with respect to $u_{\mathrm{x}}(t)$, $u_{\mathrm{y}}(t)$ and $u_0(t)$ due to the normally low value of branch inductances.

$$u_{\mathrm{xy}} = \left(\underbrace{u_{\mathrm{gx}}(t) - L_{\mathrm{x}}\frac{\mathrm{d}i_{\mathrm{x}}(t)}{\mathrm{d}t}}_{u_{\mathrm{x}}(t)}\right) - \left(\underbrace{u_{\mathrm{gy}}(t) + L_{\mathrm{y}}\frac{\mathrm{d}i_{\mathrm{y}}(t)}{\mathrm{d}t}}_{u_{\mathrm{y}}(t)}\right) - u_0(t) \tag{1}$$

$$i_{\mathrm{xy}} = \frac{1}{3}i_{\mathrm{x}}(t) + \frac{1}{3}i_{\mathrm{y}}(t) + i_{\mathrm{circ_{xy}}}(t) \tag{2}$$

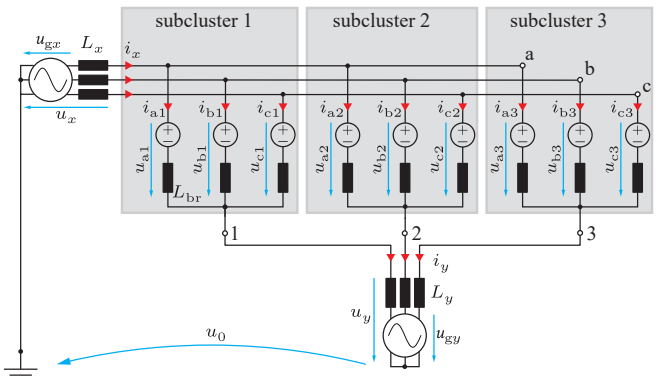

Fig. 3. Illustration of the M3C using a controlled voltage source as equivalent model for the string of cells. Adopted current and voltage directions are used throughout the rest of this paper. Values associated with the input grid get the subscripts $[a, b, c]$ and the ones associated with the output grid the subscripts $[1, 2, 3]$.

This article has been accepted for publication in IEEE Transactions on Power Electronics. This is the author's version which has not been fully edited and content may change prior to final publication. Citation information: DOI 10.1109/TPEL.2022.3215734

The branch power expression is obtained by the multiplication of (1) and (2):

$$\begin{aligned} p_{\mathrm{xy}} =& \left(u_{\mathrm{x}}(t) - u_{\mathrm{y}}(t) - u_0(t)\right)\left(\frac{1}{3}i_{\mathrm{x}}(t) + \frac{1}{3}i_{\mathrm{y}}(t) + i_{\mathrm{circ_{xy}}}(t)\right) \\ =& \frac{1}{3}\underbrace{u_{\mathrm{x}}(t)i_{\mathrm{x}}(t)}_{\substack{\omega_\Sigma=2\omega_{\mathrm{x}}\\ \omega_\Delta=0}} - \frac{1}{3}\underbrace{u_{\mathrm{y}}(t)i_{\mathrm{x}}(t)}_{\substack{\omega_\Sigma=\omega_{\mathrm{y}}+\omega_{\mathrm{x}}\\ \omega_\Delta=\omega_{\mathrm{y}}-\omega_{\mathrm{x}}}} - \frac{1}{3}\underbrace{u_0(t)i_{\mathrm{x}}(t)}_{\substack{\omega_\Sigma=\omega_0+\omega_{\mathrm{x}}\\ \omega_\Delta=\omega_0-\omega_{\mathrm{x}}}} \\ &+ \frac{1}{3}\underbrace{u_{\mathrm{x}}(t)i_{\mathrm{y}}(t)}_{\substack{\omega_\Sigma=\omega_{\mathrm{x}}+\omega_{\mathrm{y}}\\ \omega_\Delta=\omega_{\mathrm{x}}-\omega_{\mathrm{y}}}} - \frac{1}{3}\underbrace{u_{\mathrm{y}}(t)i_{\mathrm{y}}(t)}_{\substack{\omega_\Sigma=2\omega_{\mathrm{y}}\\ \omega_\Delta=0}} - \frac{1}{3}\underbrace{u_0(t)i_{\mathrm{y}}(t)}_{\substack{\omega_\Sigma=\omega_0+\omega_{\mathrm{y}}\\ \omega_\Delta=\omega_0-\omega_{\mathrm{x}}}} \\ &+ \underbrace{u_{\mathrm{x}}(t)i_{\mathrm{circ_{xy}}}(t)}_{\substack{\omega_\Sigma=\omega_{\mathrm{x}}+\omega_{\mathrm{circ}}\\ \omega_\Delta=\omega_{\mathrm{x}}-\omega_{\mathrm{circ}}}} - \underbrace{u_{\mathrm{y}}(t)i_{\mathrm{circ_{xy}}}(t)}_{\substack{\omega_\Sigma=\omega_{\mathrm{y}}+\omega_{\mathrm{circ}}\\ \omega_\Delta=\omega_{\mathrm{y}}-\omega_{\mathrm{circ}}}} - \underbrace{u_0(t)i_{\mathrm{circ_{xy}}}(t)}_{\substack{\omega_\Sigma=\omega_0+\omega_{\mathrm{circ}}\\ \omega_\Delta=\omega_0-\omega_{\mathrm{circ}}}} \end{aligned} \tag{3}$$

The instantaneous branch power, expressed in (3), is directly proportional to the variation of the cell capacitance voltage. However, this expression includes oscillating terms with an oscillating frequency of ω_Σ and ω_Δ. The terms having an oscillating frequency different than zero are neglected in the overall cell voltage balancing action. The reason for this being that the influence of this oscillating term on the cell voltage, observed over a full period of the given oscillating frequency, is zero. Based on this development, balancing of the energy among the branches is achieved through the dc values of (3). It is however noteworthy to mention that the capacitance sizing should be done considering these oscillating terms as to make sure that neither over nor under voltage is occurring.

In (3), the two degrees of freedom are the zero sequence voltage $u_0(t)$ and the circulating currents $i_{\mathrm{circ_{xy}}}(t)$. If chosen carefully, they generate a dc power component allowing for balancing of the energy among the branches. The input ac system frequency, which in this case is the grid, has a frequency defined at 50 Hz and the output ac system frequency is defined by the nominal frequency of the electrical machine connected to the converter. The nominal machine frequency, defined during its design, can be optimized for a given application. This optimization falls out of the scope of this analysis and the assumption of different input and output frequencies is made, which is logical given that the M3C has been adopted exactly in these application as the best candidate [20], [21]. Thus neither input nor output frequency are a degree of freedom and the power components depending solely on these frequencies should not generate any dc power offset, leading to the following conditions:

- Input power should be equal to the output power and the losses combined:

$$\frac{1}{3}u_{\mathrm{x}}(t)i_{\mathrm{x}}(t) = \frac{1}{3}u_{\mathrm{y}}(t)i_{\mathrm{y}}(t) + P_{\mathrm{loss}}$$

- Input and output frequencies should not be equal:

$$\omega_{\mathrm{x}} \neq \omega_{\mathrm{y}}$$

The operating point of equal input and output frequencies generates additional dc branch power components. This operating point can be achieved by a specially defined circulating current references but falls out of the scope of this paper.

Following these considerations, the final expression of the branch power allowing for balancing of the energy between the branches is:

$$\begin{aligned} p_{\mathrm{xy_{bal}}} =& \frac{1}{3}u_{\mathrm{x}}(t)i_{\mathrm{circ_{xy}}}(t) - \frac{1}{3}u_{\mathrm{y}}(t)i_{\mathrm{circ_{xy}}}(t) - \frac{1}{3}u_0(t)i_{\mathrm{x}}(t) \\ &- \frac{1}{3}u_0(t)i_{\mathrm{y}}(t) - \frac{1}{3}u_0(t)i_{\mathrm{circ_{xy}}}(t) \end{aligned} \tag{4}$$

The circulating currents used for the energy balancing should not affect the terminal currents.

$$\begin{aligned} i_{\mathrm{x}}(t) =& \sum_{\mathrm{y}=1,2,3} i^*_{\mathrm{xy}}(t) \\ =& i^*_{\mathrm{x}}(t) + \underbrace{\frac{1}{3}\sum_{\mathrm{y}=1,2,3} i^*_{\mathrm{y}}(t) + \sum_{\mathrm{y}=1,2,3} i^*_{\mathrm{circ_{xy}}}(t)}_{=0} \end{aligned} \tag{5}$$

$$\begin{aligned} i_{\mathrm{y}}(t) =& \sum_{\mathrm{x}=a,b,c} i^*_{\mathrm{xy}}(t) \\ =& i^*_{\mathrm{y}}(t) + \underbrace{\frac{1}{3}\sum_{\mathrm{x}=a,b,c} i^*_{\mathrm{x}}(t) + \sum_{\mathrm{x}=a,b,c} i^*_{\mathrm{circ_{xy}}}(t)}_{=0} \end{aligned} \tag{6}$$

With the assumption of balanced terminal currents, in both (5) and (6), the influence of the opposite terminal currents on the considered current is always equal to 0. Two main concepts, are used to ensure the sum of the circulating currents to add up to zero on the converter terminals.

The first relies on the reference frame change to the so called double-$\alpha\beta$ frame which ensures that the circulating currents generated do sum up to zero at the converter terminals [13]–[16]. This reference frame transformation generates four currents which, independent of their amplitude and phase angle, always sum up to zero on the converter terminals. Converting the initial energy reference to the double-$\alpha\beta$ frame and using these four previously mentioned currents to fulfill the energy reference, ensures proper energy balancing.

The second concept does not rely on a reference frame change, but modifies the circulating current reference for each branch in a way to ensure the condition above [17], [18]. The nine branch energy references are generated separately, and only the resulting branch current fulfilling this reference is modified as to sum up to zero on the converter terminals. This concept is used for both the second and the third methods compared in this work. Even though these two methods are said to belong to the same reference modification concept, mapping of the original circulating current references is done in a different way. This affects the converter balancing dynamics as shown in section IV.

III. Control performance comparison

Generally when both input and output terminal voltages are present, which is the case for most of the converters operating points, energy balancing between the branches is achieved through the use of circulating currents rather than using the zero sequence voltage. For this reason, the comparison of the three methods is carried out under the assumption that the energy balancing is achieved through the use of circulating

This article has been accepted for publication in IEEE Transactions on Power Electronics. This is the author's version which has not been fully edited and content may change prior to final publication. Citation information: DOI 10.1109/TPEL.2022.3215734

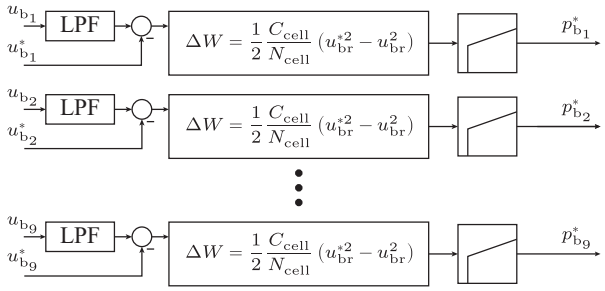

Fig. 4. Implementation of the energy PI controllers used for the energy balancing power reference calculation. Method 1 transforms the obtained power references into the double-$\alpha\beta 0$ frame and generates the current references in this new frame. Methods 2 and 3 however compute the current reference without modifying the obtained power references and modify only the obtained current references.

currents. Additionally the total energy controller being the same for any Voltage Source Converter (VSC) is omitted from the analysis conducted in this paper and the assumption is made that the overall energy within the converter is following the given setpoint.

To achieve balancing without interfering with the terminal currents, either of the two previously introduced concepts (working directly in the double-$\alpha\beta$ domain or relying on post-processing of references derived for every branch individually has to be used. This mathematical manipulation of the references aims to find the closest possible circulating current reference that achieves the required balancing action while not acting on the terminal currents. Three mathematical transformations are analyzed in the following sections, namely the double-$\alpha\beta 0$ transformation, the projection on the null space and the direct arm energy control. Through modification of the power references, the first method, allows to extract the four circulating currents which can be controlled individually. The latter method computes the required branch power for each branch separately and the resulting circulating current references do not necessarily sum up to zero at the terminals given that energy unbalances can be arbitrarily distributed over the converter. This requires a modification of the branch current references to eliminate the influence on the terminal currents.

The following subsections will illustrate the mathematical transformation applied to the branch power references aiming to balance the energy among the branches. The branch energy controller gains are set to be equal for all three methods and will thus not be further developed in this work. The structure including the PI-controllers to generate the dc branch power reference for internal balancing is shown in Fig. 4. While the nine separate branch energy controllers are used for all three methods, it is noteworthy that for the double-$\alpha\beta 0$, the control structure could be modified as to transform the initial references rather than the obtained power reference. This would allow different tuning of the PI-controllers for the different energy balancing directions. However, for a fair comparison of the reference modification applied for each method, the structure as seen in Fig. 4 is used for all three methods.

A. Method 1: double $\alpha\beta 0$ transformation [13]–[16]

The double-$\alpha\beta 0$ transformation relies, as the name suggest, on the use of the Clarke transformation matrix. Applying this transformation twice to the branch powers will lead to:

$$\begin{bmatrix} P_{\alpha\alpha} & P_{\alpha\beta} & P_{\alpha 0} \\ P_{\beta\alpha} & P_{\beta\beta} & P_{\beta 0} \\ P_{0\alpha} & P_{0\beta} & P_{00} \end{bmatrix} = \boldsymbol{C_{\alpha\beta 0}} \left(\boldsymbol{C_{\alpha\beta 0}} \begin{bmatrix} P_{\text{a}1} & P_{\text{b}1} & P_{\text{c}1} \\ P_{\text{a}2} & P_{\text{b}2} & P_{\text{c}2} \\ P_{\text{a}3} & P_{\text{b}3} & P_{\text{c}3} \end{bmatrix} \right)^{T} \tag{7}$$

$$\text{where} \quad \boldsymbol{C_{\alpha\beta 0}} = \frac{2}{3} \begin{bmatrix} 1 & \frac{-1}{2} & \frac{-1}{2} \\ 0 & \frac{\sqrt{3}}{2} & \frac{-\sqrt{3}}{2} \\ \frac{1}{2} & \frac{1}{2} & \frac{1}{2} \end{bmatrix}$$

To implement the control algorithm as explained in [16], an additional transformation is required:

$$\begin{bmatrix} P_{\text{d}1\alpha} \\ P_{\text{d}1\beta} \\ P_{\text{d}2\alpha} \\ P_{\text{d}2\beta} \end{bmatrix} = \boldsymbol{C_{\text{D}}} \begin{bmatrix} P_{\alpha\alpha} \\ P_{\alpha\beta} \\ P_{\beta\alpha} \\ P_{\beta\beta} \end{bmatrix} \tag{8}$$

$$\text{where} \quad \boldsymbol{C_{\text{D}}} = \frac{1}{2} \begin{bmatrix} 1 & 0 & 0 & 1 \\ 0 & 1 & -1 & 0 \\ 1 & 0 & 0 & -1 \\ 0 & 1 & 1 & 0 \end{bmatrix}$$

Based on these transformations, four balancing directions can be differentiated, which are defined as follows:

- Vertical: Energy balancing between the set of branches connected to the same output phase ($[P_{\text{a1,b1,c1}}], [P_{\text{a2,b2,c2}}], [P_{\text{a3,b3,c3}}]$).
- Horizontal: Energy balancing between the set of branches connected to the same input phase ($[P_{\text{a1,a2,a3}}], [P_{\text{b1,b2,b3}}], [P_{\text{c1,c2,c3}}]$).
- Diagonal 1: Energy balancing between the set of branches along the first diagonal ($[P_{\text{a1,b3,c2}}], [P_{\text{a2,b1,c1}}], [P_{\text{a3,b2,c1}}]$).
- Diagonal 2: Energy balancing between the set of branches along the second diagonal ($[P_{\text{a1,b2,c3}}], [P_{\text{a2,b3,c1}}], [P_{\text{a3,b1,c2}}]$).

To generate the given power references, a set of circulating currents in the double-$\alpha\beta 0$ frame need to be defined. Similar to (7), these currents can be defined:

$$\begin{bmatrix} i_{\alpha\alpha} & i_{\alpha\beta} & i_{\alpha 0} \\ i_{\beta\alpha} & i_{\beta\beta} & i_{\beta 0} \\ i_{0\alpha} & i_{0\beta} & i_{00} \end{bmatrix} = \boldsymbol{C_{\alpha\beta 0}} \left(\boldsymbol{C_{\alpha\beta 0}} \begin{bmatrix} i_{\text{a}1} & i_{\text{b}1} & i_{\text{c}1} \\ i_{\text{a}2} & i_{\text{b}2} & i_{\text{c}2} \\ i_{\text{a}3} & i_{\text{b}3} & i_{\text{c}3} \end{bmatrix} \right)^{T} \tag{9}$$

The currents $i_{\alpha\beta 0}$ and $i_{0\alpha\beta}$ represent the input and output terminal currents. Assuming balanced input and output terminal currents $i_{00} = 0$ holds true. Thus a total of four currents are internal to the M3C and are used for the balancing of the energy among the branches. Mathematically the same conclusion can be drawn by analyzing the structure shown in Fig 3. With a total of nine branches and six nodes, the number of independent circulating currents is defined to be 4.

Using the transformation matrix $\boldsymbol{C_D}$ as defined above, these circulating currents are transformed:

$$\begin{bmatrix} i_{\mathrm{d1}\alpha} \\ i_{\mathrm{d1}\beta} \\ i_{\mathrm{d2}\alpha} \\ i_{\mathrm{d2}\beta} \end{bmatrix} = \boldsymbol{C_D} \begin{bmatrix} i_{\alpha\alpha} \\ i_{\alpha\beta} \\ i_{\beta\alpha} \\ i_{\beta\beta} \end{bmatrix} \tag{10}$$

Using these four circulating currents, the nine power references defined in the double-$\alpha\beta$ frame can be achieved without interfering on the terminal currents.

To determine the amplitude, frequency and phase shift of the above defined circulating currents, the nine branch power expressions have to be defined in the double-$\alpha\beta$ frame. This is done in two steps:

1. Express all nine branch voltages and currents in the abc-frame as a function of the previously developed double-$\alpha\beta$ components.
2. Express all nine branch powers in the abc-frame using the previously developed double-$\alpha\beta$ current and voltage expressions.
3. Develop the branch power expressions in the double-$\alpha\beta$ frame using the transformation shown in (7) and (8)

To express the branch voltages and current using double-$\alpha\beta$ components, the inverse of the matrices $\boldsymbol{C_D}$ and $\boldsymbol{C_{\alpha\beta 0}}$ need to be defined as:

$$\boldsymbol{C_D^{-1}} = \begin{bmatrix} 1 & 0 & 1 & 0 \\ 0 & 1 & 0 & 1 \\ 0 & -1 & 0 & 1 \\ 1 & 0 & -1 & 0 \end{bmatrix} \quad \text{and} \quad \boldsymbol{C_{\alpha\beta 0}^{-1}} = \begin{bmatrix} 1 & 0 & 1 \\ \frac{-1}{2} & \frac{\sqrt{3}}{2} & 1 \\ \frac{-1}{2} & \frac{-\sqrt{3}}{2} & 1 \end{bmatrix}$$

The following development is demonstrated only for the currents, but holds true for the branch voltages as well.

$$\begin{bmatrix} i_{\alpha\alpha} \\ i_{\alpha\beta} \\ i_{\beta\alpha} \\ i_{\beta\beta} \end{bmatrix} = \boldsymbol{C_D^{-1}} \begin{bmatrix} i_{\mathrm{d1}\alpha} \\ i_{\mathrm{d1}\beta} \\ i_{\mathrm{d2}\alpha} \\ i_{\mathrm{d2}\beta} \end{bmatrix} \tag{11}$$

$$\begin{bmatrix} i_{\mathrm{a1}} & i_{\mathrm{b1}} & i_{\mathrm{c1}} \\ i_{\mathrm{a2}} & i_{\mathrm{b2}} & i_{\mathrm{c2}} \\ i_{\mathrm{a3}} & i_{\mathrm{b3}} & i_{\mathrm{c3}} \end{bmatrix} = \boldsymbol{C_{\alpha\beta 0}^{-1}} \left(\boldsymbol{C_{\alpha\beta 0}^{-1}} \begin{bmatrix} i_{\alpha\alpha} & i_{\alpha\beta} & i_{\alpha 0} \\ i_{\beta\alpha} & i_{\beta\beta} & i_{\beta 0} \\ i_{0\alpha} & i_{0\beta} & i_{00} \end{bmatrix} \right)^T \tag{12}$$

The branch voltages expressed in the double-$\alpha\beta$ frame can be simplified. The influence of the diagonal voltage components $u_{\mathrm{d1}\alpha\beta}$ and $u_{\mathrm{d2}\alpha\beta}$ is negligible on the overall branch voltage compared to the magnitude of the input and output voltages. The diagonal voltage components can thus be eliminated from the final expression. Taking this into account leads to the final nine branch power expression in the double-$\alpha\beta$ frame:

$$\begin{aligned} p_{\alpha 0} = {} & \frac{1}{6}(u_{\alpha 0} i_{\alpha 0} - u_{\beta 0} i_{\beta 0}) + \frac{1}{2}(u_{0\alpha} i_{\mathrm{d1}\alpha} + u_{0\beta} i_{\mathrm{d1}\beta}) \\ & + \frac{1}{2}(u_{0\alpha} i_{\mathrm{d2}\alpha} + u_{0\beta} i_{\mathrm{d2}\beta}) + \frac{1}{3} u_{00} i_{\alpha 0} \end{aligned} \tag{13}$$

$$\begin{aligned} p_{\beta 0} = {} & -\frac{1}{6}(u_{\alpha 0} i_{\beta 0} + u_{\beta 0} i_{\alpha 0}) - \frac{1}{2}(u_{0\alpha} i_{\mathrm{d1}\beta} + u_{0\beta} i_{\mathrm{d1}\alpha}) \\ & + \frac{1}{2}(u_{0\alpha} i_{\mathrm{d2}\beta} - u_{0\beta} i_{\mathrm{d2}\alpha}) + \frac{1}{3} u_{00} i_{\beta 0} \end{aligned} \tag{14}$$

$$\begin{aligned} p_{0\alpha} = {} & \frac{1}{6}(u_{0\alpha} i_{0\alpha} - u_{0\beta} i_{0\beta}) + \frac{1}{2}(u_{\alpha 0} i_{\mathrm{d1}\alpha} - u_{\beta 0} i_{\mathrm{d1}\beta}) \\ & + \frac{1}{2}(u_{\alpha 0} i_{\mathrm{d2}\alpha} + u_{\beta 0} i_{\mathrm{d2}\beta}) + \frac{1}{3} u_{00} i_{0\alpha} \end{aligned} \tag{15}$$

$$\begin{aligned} p_{0\beta} = {} & -\frac{1}{6}(u_{0\alpha} i_{0\beta} + u_{0\beta} i_{0\alpha}) + \frac{1}{2}(u_{\alpha 0} i_{\mathrm{d1}\beta} + u_{\beta 0} i_{\mathrm{d1}\alpha}) \\ & + \frac{1}{2}(u_{\alpha 0} i_{\mathrm{d2}\beta} - u_{\beta 0} i_{\mathrm{d2}\alpha}) + \frac{1}{3} u_{00} i_{0\beta} \end{aligned} \tag{16}$$

$$\begin{aligned} p_{\mathrm{d1}\alpha} = {} & \frac{1}{6}(u_{\alpha 0} i_{0\alpha} + u_{\beta 0} i_{0\beta}) + \frac{1}{6}(u_{0\alpha} i_{\alpha 0} + u_{0\beta} i_{\beta 0}) \\ & + \frac{1}{2}(u_{\alpha 0} i_{\mathrm{d2}\alpha} - u_{\beta 0} i_{\mathrm{d2}\beta}) + \frac{1}{2}(u_{0\alpha} i_{\mathrm{d2}\alpha} - u_{0\beta} i_{\mathrm{d2}\beta}) \\ & + u_{00} i_{\mathrm{d1}\alpha} \end{aligned} \tag{17}$$

$$\begin{aligned} p_{\mathrm{d1}\beta} = {} & \frac{1}{6}(u_{\alpha 0} i_{0\beta} - u_{\beta 0} i_{0\alpha}) - \frac{1}{6}(u_{0\alpha} i_{\beta 0} - u_{0\beta} i_{\alpha 0}) \\ & + \frac{1}{2}(u_{\alpha 0} i_{\mathrm{d2}\beta} + u_{\beta 0} i_{\mathrm{d2}\alpha}) - \frac{1}{2}(u_{0\alpha} i_{\mathrm{d2}\beta} - u_{0\beta} i_{\mathrm{d2}\alpha}) \\ & + u_{00} i_{\mathrm{d1}\beta} \end{aligned} \tag{18}$$

$$\begin{aligned} p_{\mathrm{d2}\alpha} = {} & \frac{1}{6}(u_{\alpha 0} i_{0\alpha} - u_{\beta 0} i_{0\beta}) + \frac{1}{6}(u_{0\alpha} i_{\alpha 0} - u_{0\beta} i_{\beta 0}) \\ & + \frac{1}{2}(u_{\alpha 0} i_{\mathrm{d1}\alpha} + u_{\beta 0} i_{\mathrm{d1}\beta}) + \frac{1}{2}(u_{0\alpha} i_{\mathrm{d1}\alpha} - u_{0\beta} i_{\mathrm{d1}\beta}) \\ & + u_{00} i_{\mathrm{d2}\alpha} \end{aligned} \tag{19}$$

$$\begin{aligned} p_{\mathrm{d2}\beta} = {} & \frac{1}{6}(u_{\alpha 0} i_{0\beta} + u_{\beta 0} i_{0\alpha}) + \frac{1}{6}(u_{0\alpha} i_{\beta 0} + u_{0\beta} i_{\alpha 0}) \\ & + \frac{1}{2}(u_{\alpha 0} i_{\mathrm{d1}\beta} - u_{\beta 0} i_{\mathrm{d1}\alpha}) - \frac{1}{2}(u_{0\alpha} i_{\mathrm{d1}\beta} - u_{0\beta} i_{\mathrm{d1}\alpha}) \\ & + u_{00} i_{\mathrm{d1}\beta} \end{aligned} \tag{20}$$

Each of the power components developed above include at least one of the previously defined circulating currents. In order to act on the average energy of the branch, a dc power component must be generated. Taking into account the voltage on which the circulating current act, these can be defined as to generate the required dc power reference. Summing up the resulting circulating current references, will lead to the final reference required for correct balancing of the energy. With this procedure, all internal balancing power references can be followed.

Fig. 5 shows the full load operation of the M3C using the double-$\alpha\beta$ transformation method for balancing of the energy among the branches. The voltages of the four previously defined balancing directions are shown and centered around 0 V, meaning that no imbalance in either direction is present. The oscillations of these voltages are a consequence of applying the double-$\alpha\beta$ transformation to the branch voltages without filtering. However, as stated above, balancing of the energies takes only the branch average components into account and to remove the influence of the notch filter on the dynamic responses compared hereafter, branch voltages are represented in their complete form. The amplitude of these oscillations is defined by the branch current and the cell capacitance and

This article has been accepted for publication in IEEE Transactions on Power Electronics. This is the author's version which has not been fully edited and content may change prior to final publication. Citation information: DOI 10.1109/TPEL.2022.3215734

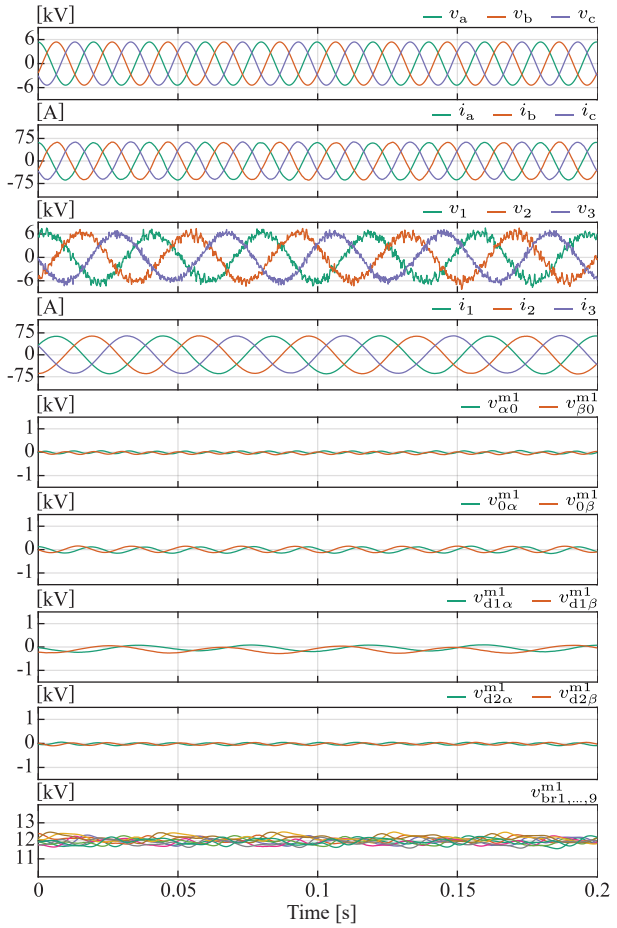

Fig. 5. Full load operation of the M3C using the double-$\alpha\beta$ transformation for balancing of the energy among the branches. Input and output terminal ac current waveforms remain uninfluenced by the circulating currents. The branch voltages remain balanced throughout the whole simulation as they all remain centered on 12 kV defined by the 8 cells charged to 1.5 kV. Their oscillations are defined by the respective branch currents and chosen branch capacitance.

should not be considered for the balancing of the energy between the branches.

B. Method 2: Null space vector projection [17]

Rather than acting on the power reference itself, the energy control method developed in [17] and presented below, modifies the circulating current references. This method is based on the principle of projecting the nine initial circulating current references onto the null space of the matrix mapping the branch current to the terminal currents. This mapping matrix is denoted by T_i in the equation below:

$$\begin{bmatrix} i_1 \\ i_2 \\ i_3 \\ i_\mathrm{a} \\ i_\mathrm{b} \\ i_\mathrm{c} \end{bmatrix} = \boldsymbol{T_\mathrm{i}} \underbrace{\begin{bmatrix} i^*_{\mathrm{a1}} & i^*_{\mathrm{b1}} & i^*_{\mathrm{c1}} & i^*_{\mathrm{a2}} & i^*_{\mathrm{b2}} & i^*_{\mathrm{c2}} & i^*_{\mathrm{a3}} & i^*_{\mathrm{b3}} & i^*_{\mathrm{c3}} \end{bmatrix}^T}_{\overrightarrow{I^*_\mathrm{b}}} \tag{21}$$

Where the matrix T_i represents the mapping $\mathbb{R}^9 \rightarrow \mathbb{R}^6$ and is defined as:

$$T_\mathrm{i} = \begin{bmatrix} 1 & 1 & 1 & 0 & 0 & 0 & 0 & 0 & 0 \\ 0 & 0 & 0 & 1 & 1 & 1 & 0 & 0 & 0 \\ 0 & 0 & 0 & 0 & 0 & 0 & 1 & 1 & 1 \\ 1 & 0 & 0 & 1 & 0 & 0 & 1 & 0 & 0 \\ 0 & 1 & 0 & 0 & 1 & 0 & 0 & 1 & 0 \\ 0 & 0 & 1 & 0 & 0 & 1 & 0 & 0 & 1 \end{bmatrix} \tag{22}$$

All the vectors $\overrightarrow{I_\mathrm{b}}$ that are mapped to zero ($T_\mathrm{i}\overrightarrow{I_\mathrm{b}} = 0$) represent branch currents which do not impact either input not output terminal currents. The vectors with this property represent the null space of T_i which is labeled as $\ker(T_\mathrm{i})$.

This balancing method relies on projecting the initial branch current references $\overrightarrow{I^*_\mathrm{b}}$ for which $T_\mathrm{i}\overrightarrow{I^*_\mathrm{b}} \neq 0$ onto the null space of T_i. This projection results in a modified set of branch current references $\overrightarrow{I^\mathrm{m}_\mathrm{b}}$ for which $T_\mathrm{i}\overrightarrow{I^\mathrm{m}_\mathrm{b}} = 0$. To allow a projection of $\overrightarrow{I^*_\mathrm{b}}$ on $\ker(T_\mathrm{i})$, the basis vectors of this space have to be defined. Finding these base vectors constitutes the core of this balancing method. The decomposition of the mapping matrix T_i using the Singular Value Decomposition (SVD) as explained in [22] and similar to the development for the MMC done in [12] allows the extraction of the required base vectors. This decomposition can be written as:

$$T_\mathrm{i} = \mathrm{U} \times \Sigma \times \mathrm{V}^\mathrm{T}, \tag{23}$$

which can be expressed as:

$$T_\mathrm{i} = \begin{bmatrix} \mathrm{U_R} & \mathrm{U_N} \end{bmatrix} \times \begin{bmatrix} \Sigma_\mathrm{R} & 0 \\ 0 & 0 \end{bmatrix} \times \begin{bmatrix} \mathrm{V^T_R} \\ \mathrm{V^T_N} \end{bmatrix}. \tag{24}$$

Based on the definition of the SVD and the definition of base vectors representing a space, it can be shown that $\mathrm{V_N}$ constitutes the basis of $\ker(T_\mathrm{i})$. Projecting the initial branch current references on this base is done using:

$$\overrightarrow{I^m_\mathrm{b}} = \mathrm{V_N}\mathrm{V^T_N}\overrightarrow{I^*_\mathrm{b}} \tag{25}$$

For the mapping matrix defined above, the base vectors are:

$$\mathrm{V_N} = \begin{bmatrix} \frac{1}{2} & \frac{1}{2\sqrt{3}} & \frac{1}{2\sqrt{3}} & \frac{1}{6} \\ 0 & -\frac{1}{\sqrt{3}} & 0 & -\frac{1}{3} \\ -\frac{1}{2} & \frac{1}{2\sqrt{3}} & -\frac{1}{2\sqrt{3}} & \frac{1}{6} \\ 0 & 0 & -\frac{1}{\sqrt{3}} & -\frac{1}{3} \\ 0 & 0 & 0 & \frac{2}{3} \\ 0 & 0 & \frac{1}{\sqrt{3}} & -\frac{1}{3} \\ -\frac{1}{2} & -\frac{1}{2\sqrt{3}} & \frac{1}{2\sqrt{3}} & \frac{1}{6} \\ 0 & \frac{1}{\sqrt{3}} & 0 & -\frac{1}{3} \\ \frac{1}{2} & -\frac{1}{2\sqrt{3}} & -\frac{1}{2\sqrt{3}} & \frac{1}{6} \end{bmatrix} \tag{26}$$

Applying this matrix to the initial set of branch current references results in the following modified reference:

$$\begin{aligned} i^{\mathrm{m}}_{\mathrm{circ}_{xy}} =& i^{*}_{\mathrm{circ}_{xy}} - \frac{1}{3}\left(\sum_{k=a,b,c} i^{*}_{\mathrm{circ}_{ky}}\right) \\ & - \frac{1}{3}\left(\sum_{j=1,2,3} i^{*}_{\mathrm{circ}_{xj}}\right) + \frac{1}{9}\left(\sum_{\substack{k=a,b,c \\ j=1,2,3}} i^{*}_{\mathrm{circ}_{kj}}\right) \end{aligned} \tag{27}$$

The initial branch power reference required to achieve branch energy balancing is used to define the initial branch current reference. For each branch this current reference is divided into two parts, one acting with the grid voltages to achieve horizontal balancing and another one at load frequency to achieve vertical balancing. These initial branch current references are defined as:

$$i^{*}_{\mathrm{circ}_{xy_h}} = \frac{2P^{*}_{xy}}{\hat{V}^2_x} v_x(t) \tag{28}$$

$$i^{*}_{\mathrm{circ}_{xy_v}} = \frac{2P^{*}_{xy}}{\hat{V}^2_y} v_y(t) \tag{29}$$

The implementation includes the initial definition of the branch currents as expressed in (28) and (29). These references are multiplied by $\mathrm{V_N V_N^T}$, using the matrix $\mathrm{V_N}$ as defined in (26), which corresponds to (27).

From (4) it is known that the branch energy average is affected by the dc power components within the branch. The above developed horizontal circulating current reference creates a dc power component only using the input terminal voltages. Multiplying (27) by the respective input terminal voltage present in the given branch yields the dc power component which enables balancing of the energy. The resulting dc power which contributes to the horizontal balancing of the energy can be calculated for each branch as:

$$\begin{aligned} \overline{P^{\mathrm{m2}}_{\mathrm{h}xy}} &= i^{\mathrm{m}}_{\mathrm{circ}_{xy_h}} v_x(t) \\ &= \frac{4}{9}P^{*}_{xy} + \frac{1}{9}\sum_{\substack{k=a,b,c \\ k\neq x}} P^{*}_{ky} - \frac{2}{9}\sum_{\substack{j=1,2,3 \\ j\neq y}} P^{*}_{xj} \\ &\quad - \frac{1}{18}\sum_{\substack{k=a,b,c\neq x \\ j=1,2,3\neq y}} P^{*}_{kj}. \end{aligned} \tag{30}$$

Similarly, the same development can be done for the vertical energy balancing using the load voltages:

$$\begin{aligned} \overline{P^{\mathrm{m2}}_{\mathrm{v}xy}} &= i^{\mathrm{m}}_{\mathrm{circ}_{xy_v}} v_y(t) \\ &= \frac{4}{9}P^{*}_{xy} + \frac{1}{9}\sum_{\substack{j=1,2,3 \\ j\neq y}} P^{*}_{xj} - \frac{2}{9}\sum_{\substack{k=a,b,c \\ k\neq x}} P^{*}_{ky} \\ &\quad - \frac{1}{18}\sum_{\substack{k=a,b,c\neq x \\ j=1,2,3\neq y}} P^{*}_{kj} \end{aligned} \tag{31}$$

The final branch power acting on the average branch energy is the sum of both the horizontal and the vertical component.

$$\overline{P^{\mathrm{m2}}_{xy}} = \overline{P^{\mathrm{m2}}_{\mathrm{h}xy}} + \overline{P^{\mathrm{m2}}_{\mathrm{v}xy}} \tag{32}$$

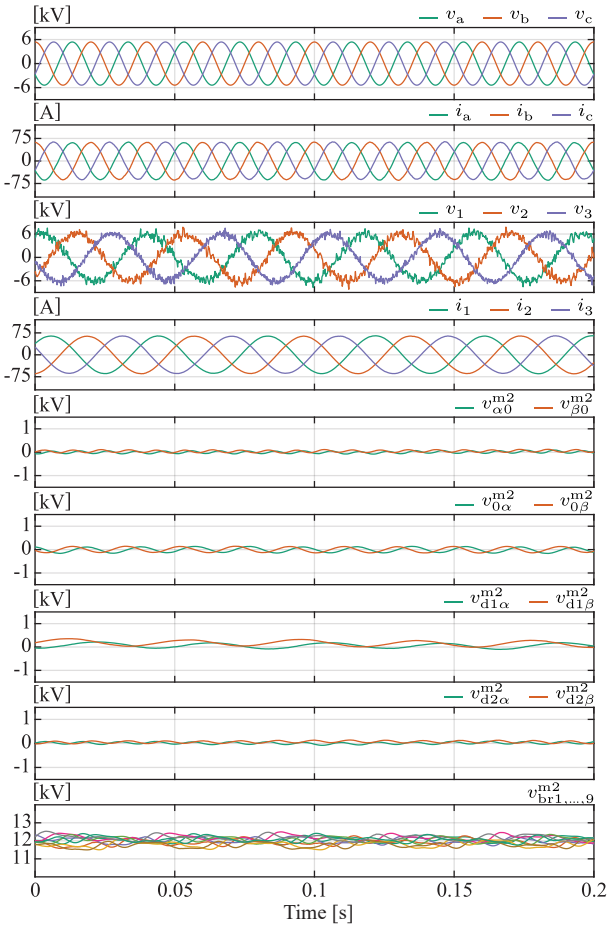

Fig. 6. Full load operation of the M3C using the null space vector projection for balancing of the energy among the branches. Input and output terminal ac current waveforms remain uninfluenced by the circulating currents. The branch voltages remain balanced throughout the whole simulation while their oscillations are defined by the respective branch currents and chosen branch capacitance.

Fig. 6 demonstrates the proper operation of this method under full load operation as overall energy balancing among the converter is achieved.

C. Method 3: direct arm energy control [18]

Similar to the second method described above, the direct arm energy control modifies the circulating current references rather than the power reference as is the case for the first method. The principle of this method relies on subtracting the average of all circulating currents references from the branches connected to the same input and output phases to the given branch circulating current reference.

As the method is developed in the abc frame, the same balancing directions, namely the vertical and the horizontal direction can be defined. While the diagonal direction defined in the double-$\alpha\beta 0$ frame is not explicitly defined in the initial set of current references, they are implicitly included which is shown when converted to the double-$\alpha\beta 0$ frame, as will be seen later on.

Horizontal balancing is achieved by acting on the input grid voltage component present in the branch voltage expression,

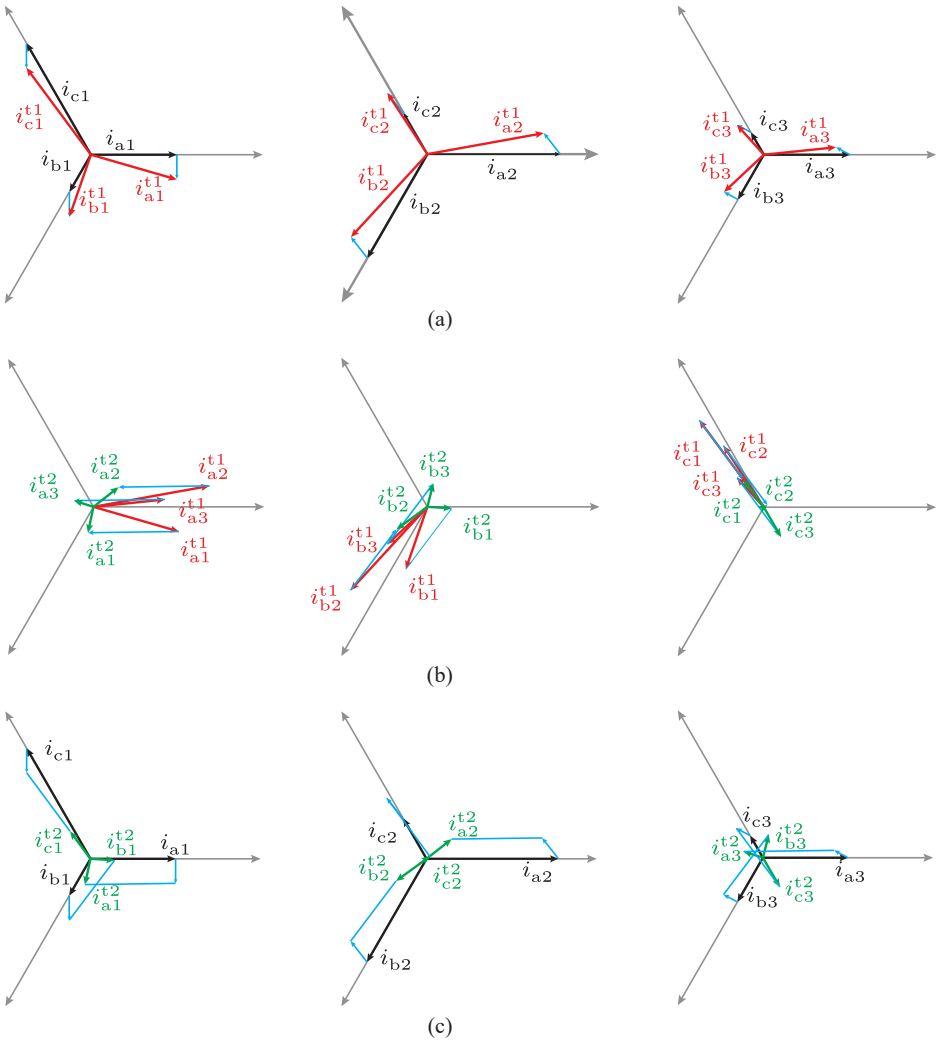

Fig. 7. Modification of the circulating current reference. (a) showing the original circulating current reference in black as well as the first modification step colored in red. (b) shows the second modification stage with the initial reference in red and the final reference in orange. (c) shows a comparison between the initial reference and the modified one.

and the initial branch current reference for each of the nine branches is equal to the one presented in method 2:

$$i_{\mathrm{circ}_{xy_h}} = \frac{2P^*_{xy}}{\hat{V}_x^2} v_x(t) \tag{33}$$

As this reference is generated directly from the power reference, while energy unbalances within the converter can be arbitrarily distributed, it cannot be guaranteed that the terminal currents remain uninfluenced. As shown in [18], the influence on the input grid terminals can be eliminated by modifying the initial circulating current references using:

$$i^{\mathrm{t_1}}_{\mathrm{circ}_{xy_h}} = i_{\mathrm{circ}_{xy_h}} - \frac{1}{3}\left(\sum_{k=a,b,c} i_{\mathrm{circ}_{ky_h}}\right) \tag{34}$$

While the modification of the initial reference shown above ensures no influence on the input grid terminals, there is no guarantee that the output terminal currents remain uninfluenced. For this reason, an additional modification of the reference is required:

$$i^{\mathrm{t_2}}_{\mathrm{circ}_{xy_h}} = i^{\mathrm{t_1}}_{\mathrm{circ}_{xy_h}} - \frac{1}{3}\left(\sum_{j=1,2,3} i^{\mathrm{t_1}}_{\mathrm{circ}_{xj_h}}\right) \tag{35}$$

While this method uses a seemingly different transformation than method 2, when comparing the final references of both methods in the horizontal direction, they lead to the same final expression.

Fig. 7 provides an illustration of the two modifications expressed above as well as a comparison between the initial and final references.

Due to the two modifications illustrated above, the final circulating current reference of the given balancing direction does not alter the terminal currents of the M3C. As the final horizontal branch current reference is equal to the one of the previous method, the resulting dc branch power in the

horizontal direction will have the same expression as well:

$$\begin{aligned}\overline{P^{\mathrm{m3}}_{\mathrm{h}xy}} &= i^{\mathrm{t2}}_{\mathrm{circ}_{xy_h}} v_x(t) \\ &= \frac{2}{9}P^*_{xy} + \frac{1}{18}\sum_{\substack{k=a,b,c\\k\neq x}} P^*_{ky} - \frac{1}{9}\sum_{\substack{j=1,2,3\\j\neq y}} P^*_{xj} \\ &\quad - \frac{1}{36}\sum_{\substack{k=a,b,c\neq x\\j=1,2,3\neq y}} P^*_{kj}\end{aligned} \tag{36}$$

Vertical balancing is achieved through circulating currents acting on the load terminal voltages. Assuming that the total energy control works properly, averaging the power reference of all branches connected to the same input terminal eliminates the influence on the load terminals. This leads to the initial circulating current reference for vertical balancing:

$$i_{\mathrm{circ}_{xy_v}} = \frac{v_y(t)}{3\hat{V}_y^2}\sum_{j=1,2,3} P_{xj} \tag{37}$$

To eliminate the impact on the input terminals of the M3C, the same procedure as for the horizontal balancing is used. A single modification is enough to eliminate influence on all terminals, due to the initial definition of the circulating current:

$$i^{\mathrm{t1}}_{\mathrm{circ}_{xy_v}} = i_{\mathrm{circ}_{xy_v}} - \frac{1}{3}\left(\sum_{k=a,b,c} i_{\mathrm{circ}_{ky_v}}\right) \tag{38}$$

A dc power component is achieved through the multiplication of the vertical circulating currents with the load terminal voltages present in the branches. This multiplication leads to the following dc power expression:

$$\begin{aligned}\overline{P^{\mathrm{m3}}_{\mathrm{v}xy}} &= i^{\mathrm{t1}}_{\mathrm{circ}_{xy_v}} v_y(t) \\ &= \frac{1}{9}\sum_{j=1,2,3} P^*_{xj} - \frac{1}{18}\sum_{\substack{k=a,b,c\neq x\\j=1,2,3}} P^*_{kj}\end{aligned} \tag{39}$$

The final branch power acting on the average branch energy is the sum of both the horizontal and the vertical component as defined for method 2 in (31).

$$\overline{P^{\mathrm{m3}}_{xy}} = \overline{P^{\mathrm{m3}}_{\mathrm{h}xy}} + \overline{P^{\mathrm{m3}}_{\mathrm{v}xy}} \tag{40}$$

Fig. 8 shows the full load operation of the M3C using the above described direct arm energy control and demonstrating its proper energy balancing performance.

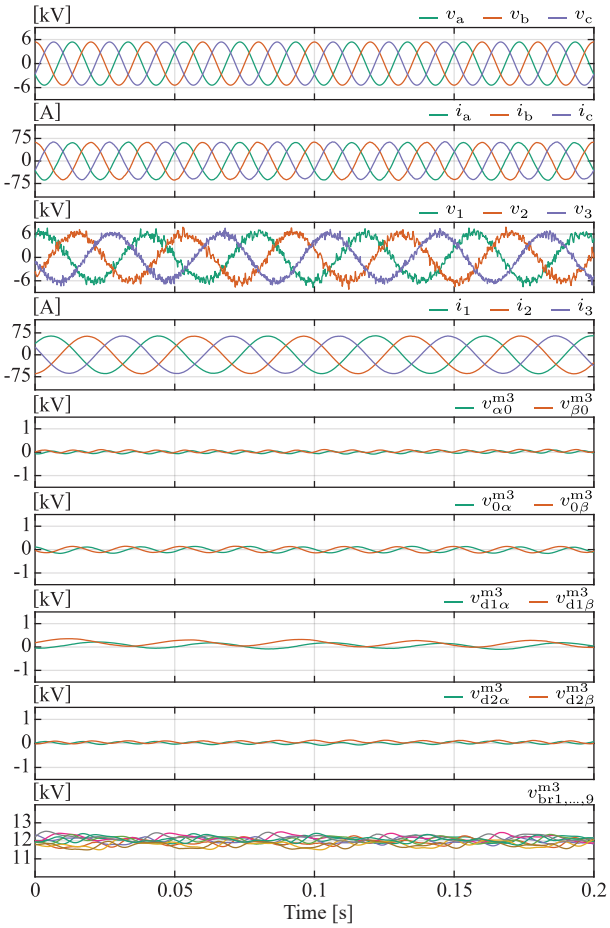

Fig. 8. Full load operation of the M3C using the direct arm energy control for balancing of the energy among the branches. Input and output terminal ac current waveforms remain uninfluenced by the circulating currents. The branch voltages remain balanced throughout the whole simulation while their oscillations are defined by the respective branch currents and chosen branch capacitance.

IV. Performance Comparison

A. Dc power reference comparison

To enable a comparison between the methods, the frame in which they are analyzed should be the same. Additionally, equal controller gains are required to allow a fair comparison. The double-$\alpha\beta$ method is developed in the double-$\alpha\beta$ frame, whereas the null space projection method and the direct arm energy control are in the abc frame. Transforming the latter method into the double-$\alpha\beta$ requires the development of the equations (7) and (8).

$$P_{\alpha 0} = \frac{1}{9}\left(2\sum_{j=1,2,3} P_{\mathrm{a}j} - \sum_{\substack{k=b,c\\j=1,2,3}} P_{kj}\right) \tag{41}$$

$$P_{\beta 0} = \frac{1}{3\sqrt{3}}\left(\sum_{j=1,2,3} P_{\mathrm{b}j} - \sum_{j=1,2,3} P_{\mathrm{c}j}\right) \tag{42}$$

$$P_{0\alpha} = \frac{1}{9}\left(2\sum_{k=a,b,c} P_{k1} - \sum_{\substack{k=a,b,c\\j=2,3}} P_{kj}\right) \tag{43}$$

$$P_{0\beta} = \frac{1}{3\sqrt{3}}\left(\sum_{k=a,b,c} P_{k2} - \sum_{k=a,b,c} P_{k3}\right) \tag{44}$$

$$P_{\mathrm{d}1\alpha} = \frac{1}{9}\left(3\left(P_{\mathrm{a}1} + P_{\mathrm{b}2} + P_{\mathrm{c}3}\right) - \sum_{\substack{k=a,b,c\\j=1,2,3}} P_{kj}\right) \tag{45}$$

$$P_{\mathrm{d1}\beta} = \frac{1}{3\sqrt{3}} \left(P_{\mathrm{a2}} + P_{\mathrm{b3}} + P_{\mathrm{c1}} - P_{\mathrm{a3}} - P_{\mathrm{b1}} - P_{\mathrm{c2}}\right) \quad (46)$$

$$P_{\mathrm{d2}\alpha} = \frac{1}{9} \left(3\left(P_{\mathrm{a1}} + P_{\mathrm{b3}} + P_{\mathrm{c1}}\right) - \sum_{\substack{k=a,b,c \\ j=1,2,3}} P_{kj} \right) \quad (47)$$

$$P_{\mathrm{d2}\beta} = \frac{1}{3\sqrt{3}} \left(P_{\mathrm{a2}} + P_{\mathrm{b1}} + P_{\mathrm{c3}} - P_{\mathrm{a3}} - P_{\mathrm{b2}} - P_{\mathrm{c1}}\right) \quad (48)$$

The first method, using the double-$\alpha\beta$ transformation, fulfills the exact required power reference as explained in the section above using (13) to (20). For the second method substituting (31) into (41) - (48) transforms the power references into the double-$\alpha\beta$ frame, whereas for the third method the same procedure is done using (40). The resulting power can be expressed as the multiplication of a scaling factor and the power expression of method 1:

$$\begin{bmatrix} P_{\mathrm{v}}^{\mathrm{m2,m3}} \\ P_{\mathrm{h}}^{\mathrm{m2,m3}} \\ P_{\mathrm{d1}}^{\mathrm{m2,m3}} \\ P_{\mathrm{d2}}^{\mathrm{m2,m3}} \end{bmatrix} = \begin{bmatrix} k_{\mathrm{v}}^{\mathrm{m2,m3}} & 0 & 0 & 0 \\ 0 & k_{\mathrm{h}}^{\mathrm{m2,m3}} & 0 & 0 \\ 0 & 0 & k_{\mathrm{d1}}^{\mathrm{m2,m3}} & 0 \\ 0 & 0 & 0 & k_{\mathrm{d2}}^{\mathrm{m2,m3}} \end{bmatrix} \begin{bmatrix} P_{\mathrm{v}}^{\mathrm{m1}} \\ P_{\mathrm{h}}^{\mathrm{m1}} \\ P_{\mathrm{d1}}^{\mathrm{m1}} \\ P_{\mathrm{d2}}^{\mathrm{m1}} \end{bmatrix} \quad (49)$$

A scaling factor $k = 1$ means that both methods have equal performances in the given direction. Table I, shows the scaling factor for each of the defined balancing directions. Based on the branch energy variation established in the first section, this scaling factor affects the dc power component within the branches to achieve balancing in the given direction. Analyzing table I shows that all three methods generate the same dc power component in the vertical as well as in the horizontal direction, demonstrating equal performance of all three methods in these balancing directions.

A closer analysis of the branch power equations of method 2 converted to the double-$\alpha\beta$ frame shows that even without explicitly defining the diagonal directions, achieves the same performance along these axes compared to method 1. However, method 3 developed similarly to method 2 in abc frame, shows a reduced dc power component in the diagonal directions. Both methods generate the same horizontal power component as shown in (30) and (36), thus they differentiate each other only by their vertical power component. This demonstrates that the modification of the circulating currents in the vertical direction for method 2 influences the diagonal balancing directions while the initially defined vertical direction $\overline{P_{\mathrm{v}xy}^{\mathrm{m3}}}$ acts only on the vertical direction.

As method 3 defines only the horizontal and vertical balancing directions explicitly, introducing a gain on the current reference to achieve equal diagonal balancing performance, will influence the horizontal direction. This leads to an excess in power reference in the horizontal direction. Thus method 3 cannot achieve equal performance compared to methods 1 and 2, since no gain can be explicitly defined for diagonal directions.

TABLE I: Scaling coefficient for the comparison of method 1, method 2 and method 3.

	Scaling coefficients		
Balancing direction	Method 1	Method 2	Method 3
Vertical ($P_{\alpha 0}, P_{\beta 0}$)	1	1	1
Horizontal ($P_{0\alpha}, P_{0\beta}$)	1	1	1
Diagonal 1 ($P_{\mathrm{d1}\alpha}, P_{\mathrm{d1}\beta}$)	1	1	$1/2$
Diagonal 2 ($P_{\mathrm{d2}\alpha}, P_{\mathrm{d2}\beta}$)	1	1	$1/2$

While table I compares the dc power references resulting from the three methods in the four directions, it does not reveal any information about the actual amplitude and phase shift of the circulating currents. While methods 1 and 2 achieve equal performance in all four balancing directions, the circulating currents achieving this power components are different for these methods as will be demonstrated in the following section.

B. Circulating current scaling

In the double-$\alpha\beta$ frame, the currents used for balancing of the energy among the branches of the converter are $i_{\mathrm{d1}\alpha,\mathrm{d1}\beta}$ and $i_{\mathrm{d2}\alpha,\mathrm{d2}\beta}$. For each of the four previously defined balancing directions, these currents can be defined as to generate the required power reference. This leads to the following equations:

$$i_{\mathrm{d1}} = k_{\mathrm{i_{d1_v}}} i_{\mathrm{d1_v}} + k_{\mathrm{i_{d1_h}}} i_{\mathrm{d1_h}} + k_{\mathrm{i_{d1_{d1}}}} i_{\mathrm{d1_{d1}}} + k_{\mathrm{i_{d1_{d1}}}} i_{\mathrm{d1_{d2}}} \quad (50)$$

$$i_{\mathrm{d2}} = k_{\mathrm{i_{d2_v}}} i_{\mathrm{d2_v}} + k_{\mathrm{i_{d2_h}}} i_{\mathrm{d2_h}} + k_{\mathrm{i_{d2_{d1}}}} i_{\mathrm{d2_{d1}}} + k_{\mathrm{i_{d2_{d1}}}} i_{\mathrm{d2_{d2}}} \quad (51)$$

Each of the two diagonal currents above include components of both input and output ac frequencies, and table II shows the value of the coefficients for each method. Analyzing the equations (13) to (20), it can be seen that no power expression includes all four circulating currents. The currents that are not present and thus cannot be used for balancing in a given direction are the same for all three methods and marked by a black cell in table II. To achieve an accurate dc power reference in the branch for a given balancing directions, the sum of all the circulating current coefficients of that given direction should sum up to 1.

Analyzing the table for method 1, it is shown that not only do all the columns of the four direction always sum up to 1, but additionally it is shown that the contribution of the currents for a given direction can be modified. This is a significant advantage considering the Low Voltage Ride Through (LVRT) capabilities. In this case, the input ac voltage drops down to nearly 0, thus the frequency component ω_x is significantly reduced in all the branches. For the vertical direction, the LVRT does not reduce the balancing action as this balancing direction requires only the presence of load voltage frequencies in the branch. The horizontal direction cannot be controlled with neither of the methods as the only possibility is to act on the grid frequencies which are not present in the LVRT. For the first diagonal balancing, the possibility of choosing the frequency component of the circulating current allows to achieve the required dc power component by choosing $k_{\mathrm{d1}}^{\mathrm{m1}} = 1$, in which case only the load frequency is used. Similarly for the second diagonal, where $k_{\mathrm{d2}}^{\mathrm{m1}} = 1$ achieves the required power reference using the load frequency. In normal operation, the freedom to choose the frequency component of the circulating currents allows to reduce their amplitude by considering the branch voltage amplitudes at the given frequencies.

TABLE II: Circulating current scaling coefficient for each of the frequency component of the available circulating currents. Black cells indicate the impossibility of using this component for the given balancing direction and a red cell highlights the impossibility of creating this component for a given method. This table compares the current coefficients for the three methods compared in this paper.

			Current Scaling Coefficients			
	Curr.	Freq.	Ver	Hor	Dia. 1	Dia 2
Meth 1	$\lvert I_{\mathrm{d1}}\rvert$	ω_x		$1-k_{\mathrm{hor}}^{\mathrm{m1}}$		$1-k_{\mathrm{d2}}^{\mathrm{m1}}$
		ω_y	$1-k_{\mathrm{ver}}^{\mathrm{m1}}$			$k_{\mathrm{d2}}^{\mathrm{m1}}$
	$\lvert I_{\mathrm{d2}}\rvert$	ω_x		$k_{\mathrm{hor}}^{\mathrm{m1}}$	$1-k_{\mathrm{d1}}^{\mathrm{m1}}$	
		ω_y	$k_{\mathrm{ver}}^{\mathrm{m1}}$		$k_{\mathrm{d1}}^{\mathrm{m1}}$	
Meth 2	$\lvert I_{\mathrm{d1}}\rvert$	ω_x		0.5		0.5
		ω_y	0.5			0.5
	$\lvert I_{\mathrm{d2}}\rvert$	ω_x		0.5	0.5	
		ω_y	0.5		0.5	
Meth 3	$\lvert I_{\mathrm{d1}}\rvert$	ω_x		0.5		0.5
		ω_y	0.5			0
	$\lvert I_{\mathrm{d2}}\rvert$	ω_x		0.5	0.5	
		ω_y	0.5		0	

Taking the example of method 2 in any of the four defined directions, it can be seen that the in all four cases, the sum of the coefficients is equal to 1, thus achieving the required branch power reference to balance in the given directions. In contrast to method 1 however, the method 2 does not have any degree of freedom as to chose the frequency of the circulating currents. Consequently during a loss of the grid voltage, the balancing in both diagonal directions is affected as only the part acting on the load voltages contributes to generating a dc power reference in the branches which will thus be reduced by 50%. Additionally, the missing freedom to choose the frequency of the circulating currents does not allow for any circulating current amplitude optimization as is the case for the first method.

The third method shows the same reduced freedom to choose the frequency of the circulating currents demonstrated in method 2. However, as shown by the marked red cells, this method does not include any load frequency component for the diagonal balancing actions. While in normal operation, this translates into only half the required dc power component present in the branch as is shown in table I, in LVRT this means a complete loss of balancing in either of the diagonal actions as no grid frequency voltage component is present in the branches.

V. Hardware-in-the-Loop Results

A. Hardware-in-the-Loop setup

To compare both control methods above in a thorough manner, a HIL platform is used. As shown in Fig. 9, the control structure of the HIL is based on an industrial control platform. The complexity of the M3C required the splitting of the model onto multiple RT Boxes. The final setup as shown in Fig. 9 uses one RT Box for each branch, collecting the switching signals from the Control Hub (CHUB) and sends the resulting branch voltage to the application RT Box. The grid and machine model as well as the mapping of the branch voltages to mimick the M3C is implemented on the application RT Box. Further details of the model and the setup can be found in [19].

Fig. 9. HIL system for the M3C using the RT Boxes to host the simulated part of the setup as seen on the left side showing the front view of the cabinet. A total of 9 branch RT Boxes and one application RT Box are used. The industrial control structure, hosted on the back of the cabinet, uses the ABB AC800 PEC controllers.

B. Hardware-in-the-Loop test results

The dynamic response of these control algorithms can be tested in two different ways. The first one being their ability to reject an unbalance, whereas the second one is their ability to generate an imbalance. As both ways achieve the same goal, the latter one is used in this comparison.

To achieve a representative comparison between the three methods, the instance regarding terminal conditions at which the branch energy reference is modified is the same for all the methods.

The performance regarding the vertical balancing is shown in Fig. 10 (a). In a balanced operating scenario, such as shown in Fig. 8 and Fig. 5, all the branch voltage components in the double-$\alpha\beta$ frame oscillate with a mean value of 0 V, which corresponds to an equivalent branch voltage of 12 kV for all nine branches. A vertical imbalance is generated at 0.1 s, where the reference corresponding to the α component of this direction is increased to 1 kV. Transforming this imbalance into the abc frame results in a voltage reference of 13 kV for the branches a1, a2 and a3 whereas the other six branches have a reference of 1.15 kV to keep the overall charge within the converter constant. The response to this reference change is shown in green for method 1, orange for method 2 and violet for method 3. From the plot showing $v_{\alpha 0}$ no significant difference in the response of the three methods can be noticed.

Fig. 10 (b) compares the response of the three methods in the horizontal balancing direction. The reference to all the branches connected to the first output phase (a1, b1, c1) is increased by 1 kV whereas the reference for the remaining six branches is reduced to 1.15 kV. In the double-$\alpha\beta$ frame this

This article has been accepted for publication in IEEE Transactions on Power Electronics. This is the author's version which has not been fully edited and content may change prior to final publication. Citation information: DOI 10.1109/TPEL.2022.3215734

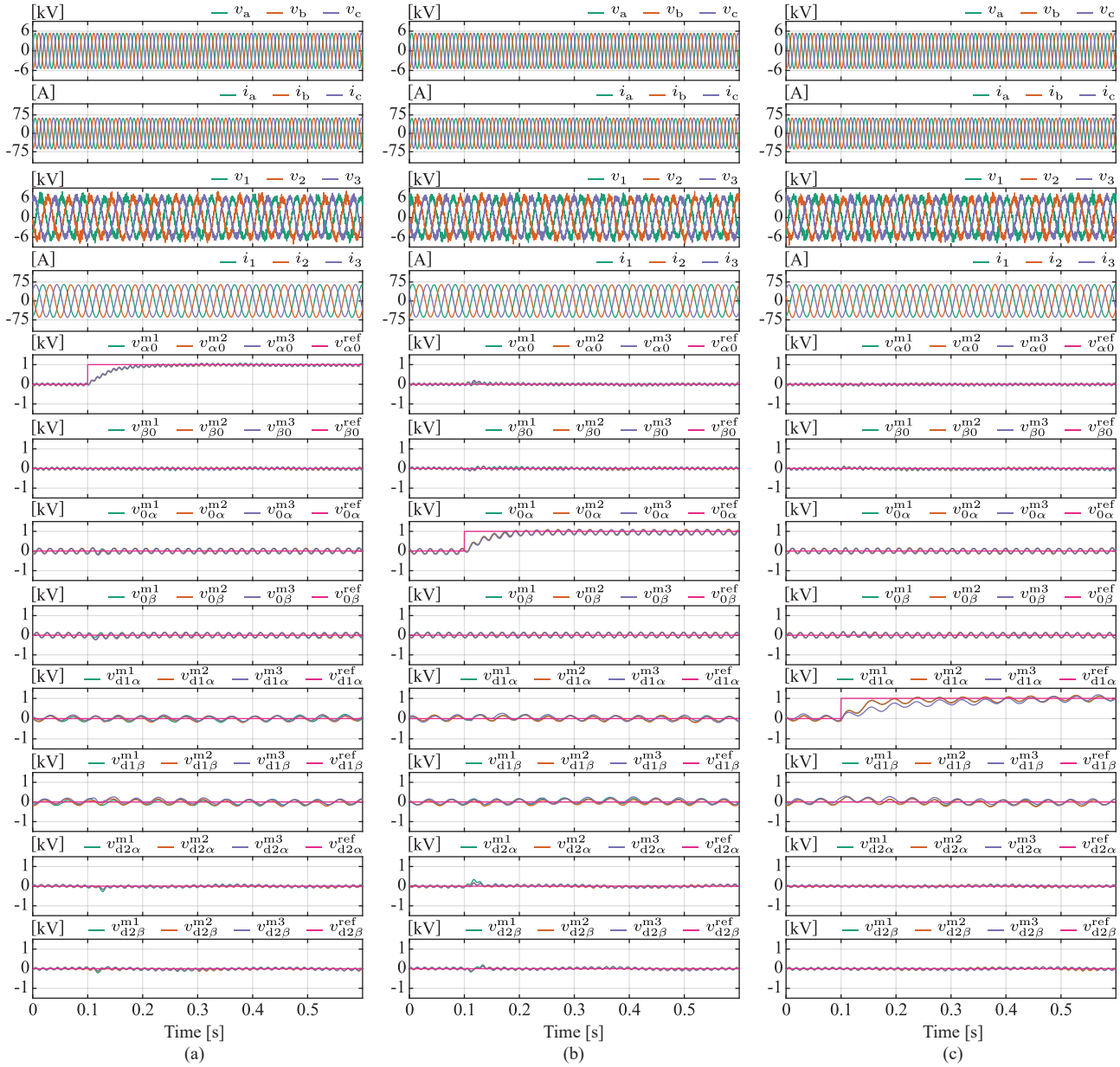

Fig. 10. RT-HIL results showing three different branch energy reference imbalances and the response of the three previously introduced methods. The subfigures show, from top to bottom, the grid voltages and currents, the machine voltages and currents, the vertical α and β branch voltages, the horizontal α and β branch voltages, the diagonal 1 α and β branch voltages as well as the diagonal 2 α and β branch voltages. The first four subfigures showing the terminal currents and voltages demonstrate unchanged waveforms regardless of the circulating currents. Part (a) shows the response of the algorithm to a vertical imbalance of 1 kV, part (b) illustrates the same for the horizontal direction and part (c) for the first diagonal.

corresponds to a 1 kV reference of the $v_{0\alpha}$ component, which can be seen in (b). Similar to the observation of the vertical imbalance, all the methods reach the required reference at the same rate.

For part (c) of Fig. 10, an imbalance along the first diagonal of the branches of the M3C is generated. Regarding the branch references, branches a1, b2 and c3 are increased to 13 kV and to keep the overall energy within the converter constant, the other six branch references are decreased to 1.15 kV. While the first and second methods reach the reference voltage within the same time as for the previous two imbalances shown in (a) and (b), method 3 requires a longer time compared to the vertical and horizontal imbalance. This observation correlates with the conclusion of theoretical development shown in Table I.

Fig 11 (a) shows the imbalance along the second diagonal, which is the last of the four defined balancing directions. For the scenario presented here, the branch references of a1, b3 and c2 are increased to 13 kV and the remaining references are decreased to 1.15 kV. For the second diagonal this transforms into a 1 kV reference which is achieved by methods 1 and 2 within the same time delay as for all the previous presented imbalances. Similar to the imbalance along the first diagonal, the third method requires also for the second diagonal imbalance more time compared to the other two

This article has been accepted for publication in IEEE Transactions on Power Electronics. This is the author's version which has not been fully edited and content may change prior to final publication. Citation information: DOI 10.1109/TPEL.2022.3215734

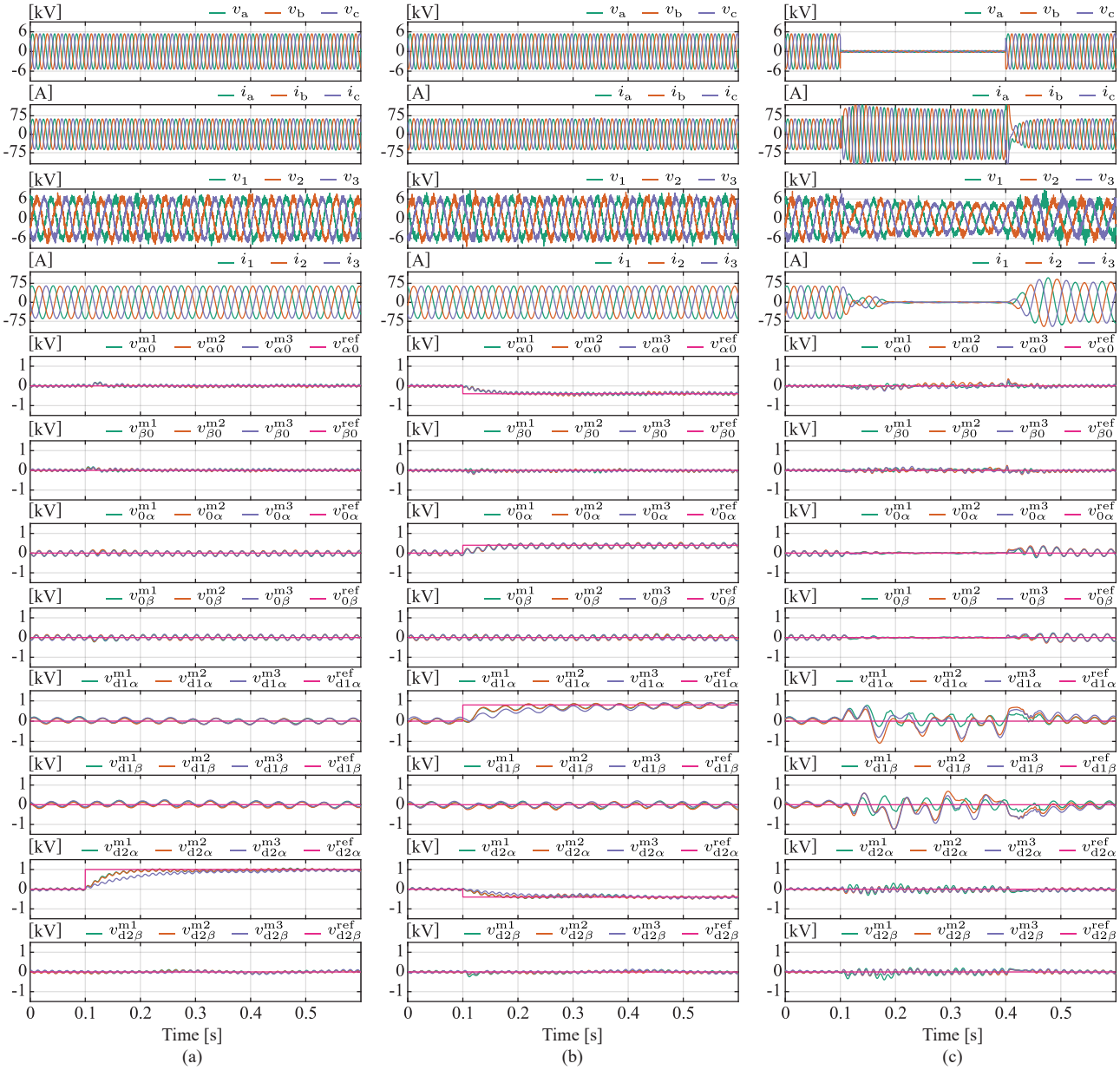

Fig. 11. RT-HIL results showing two different branch energy reference imbalances as well as the LVRT response of the three previously introduced methods. The subfigures show, from top to bottom, the grid voltages and currents, the machine voltages and currents, the vertical α and β branch voltages, the horizontal α and β branch voltages, the diagonal 1 α and β branch voltages as well as the diagonal 2 α and β branch voltages. The first four subfigures showing the terminal currents and voltages demonstrate unchanged waveforms regardless of the circulating currents. Part (a) shows the response of the algorithm to a vertical imbalance of 1 kV, part (b) illustrates the same for the horizontal direction and part (c) for the first diagonal.

methods.

A random imbalance presented in Fig 11 (b) validates all the previous conclusion drawn for the individual imbalances. Methods 1 and 2 cannot be distinguished in their performance, however they both outperform the third method in the two diagonal imbalance directions. For both the horizontal and the vertical directions, all three methods reach the required reference within the same time, thus no performance difference can be noticed.

Fig 11 (c) shows the LVRT performance of all three methods, while the converter complies with the German grid code as defined in [23]. During this scenario, neither load currents not grid voltages are present in the branch needed for horizontal balancing of all three methods. However, as no imbalance is created in this direction during the transient as seen on the $v_{0\alpha}$ and the $v_{0\beta}$ plots, no balancing action is required. As shown in table II, method 1 provides the additional degree of freedom to choose between grid or load voltages to balance in the diagonal directions. As seen in Fig 11 (c), even without grid voltage components, method 1 manages to balance the energy in the three remaining directions. Neither method 2 nor method 3 have this degree of freedom and rely on the grid voltage to achieve diagonal balancing. Method 3 relies solely on the grid voltage to achieve

diagonal balancing, thus during LVRT, no energy balancing in these direction can be achieved. Even if method 2 relies on both input and output components to achieve diagonal balancing and should thus outperform method 2 during LVRT, no significant performance difference can be observed between the two methods.

For all the imbalance scenarios shown in Fig. 10 and Fig. 11, the reference change does not generate a steady state imbalance along any other balancing direction. Even if during the transients, a small variation of the diagonal voltages can be observed, no significant difference between the three methods can be observed.

VI. Conclusion

Through the mathematical development of the main energy balancing control algorithms, this work fills existing theoretical gaps, and allows a thorough analytical comparison of all methods. While a similar study on the MMC exists [12], the performance of the methods differs for the M3C topology. In the previous study the here called method 2 had a reduced dynamic performance compared to method 1, whereas in this work, assuming normal operation, both methods perform similarly.

Fig. 12 illustrates the most important characteristics for each of the three methods. Method 1, shown in green, requires a high implementation effort due to the high amount of transformation blocks as well as the conditions to chose the optimal circulating current reference. Additionally, the implementation in the double-$\alpha\beta$ frame while allowing different control gains for different balancing directions, requires tuning of one control loop for each balancing direction. This method provides a high degree of freedom in choice of the circulating currents to generate as to balance the energy. This choice, however, requires a high amount of scenarios to be implemented as well as multiple conditions choosing among all the possible circulating current components. Method 1 however achieves the highest dynamic response during normal operating mode, thus leading to an efficient energy balance among the branches. The advantage of the high degrees of freedom of the circulating currents is the good performance during grid scenarios such as LVRT as was shown in the RT-HIL test results.

The second method, shown in blue on Fig. 12, requires an extensive knowledge of linear algebra as well as vector spaces and might not be intuitive. However, the implementation of this method is the simplest of all three analyzed methods as it only requires a single gain to get a modified current reference. During normal operation, this method achieves the same high dynamic behavior to the first method. The computation in abc frame does not allow individual tuning of the energy controllers for the four defined directions. Additionally, the simple implementation does not provide any degrees of freedom in choice of circulating current reference and as a consequence has a very low performance during LVRT.

The third method, shown in orange on Fig. 12, relies on a simple mathematical transformation which can be easily understood with a relative effort of implementation. However,

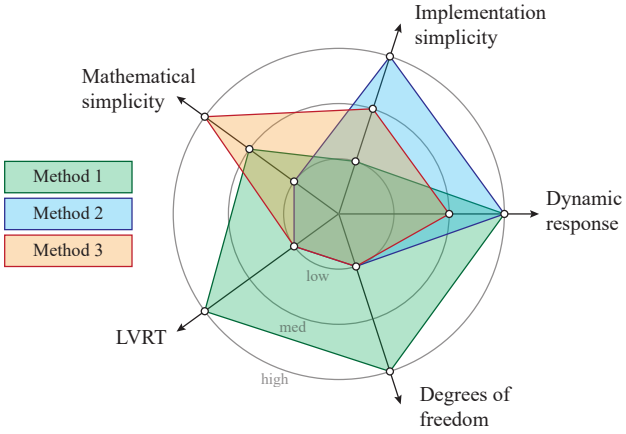

Fig. 12. Overview of the characteristics of each control method. Mathematical simplicity is defined as the ease of understanding the principle of the given method. The implementation simplicity is representative of the complexity and time investment for the implementation. The dynamic response illustrates the energy balancing performance during normal operation of the converter. The degrees of freedom demonstrate the possibility of introducing various gains for the different balancing directions as well as having the possibility of choosing the components of the circulating currents. The LVRT illustrates the energy balancing performance of the various control methods during this grid fault.

the reduced diagonal 1 and 2 balancing performance of this method results a lower dynamic response compared to the two previous methods. Similarly to method 2, the implementation in the abc frame does not allow an individual tuning of the energy controllers of the different directions. Additionally, this method does not allow any flexibility in choice of circulating currents, which translates in a poor performance during LVRT.

Each of the analyzed methods achieves balancing of the energy within the converter without affecting the terminal currents, for this reason they all fulfill the main requirement of the energy balancing algorithm. Regarding the choice of implementation, it is up to the control engineer to evaluate the trade off between the different implementations, considering the resources at disposal for the given application.

Acknowledgment

The results presented in this paper are a part of the Hydropower Extending Power System Flexibility (XFLEX HYDRO) project that has received funding from the European Union's Horizon 2020 research and innovation programme under grant agreement No 857832.

References

[1] A. Iwadachi, K. Tani, and K. Aguro, "The design of adjustable-speed pump-turbine modified from existing constant-speed on okutataragi power station," in *2016 19th International Conference on Electrical Machines and Systems (ICEMS)*, 2016, pp. 1–4.

[2] A. Vargas-Serrano, A. Hamann, S. Hedtke, C. M. Franck, and G. Hug, "Economic benefit analysis of retrofitting a fixed-speed pumped storage hydropower plant with an adjustable-speed machine," in *2017 IEEE Manchester PowerTech*, 2017, pp. 1–6.

[3] P. Bontemps, N. Hugo, and D. Dujic, "Flexibility enhancements in pumped hydro storage power plants through variable speed drives," in *IECON 2020 The 46th Annual Conference of the IEEE Industrial Electronics Society*, 2020, pp. 1820–1825.

[4] A. Christe. (). "Direct mmc for converter-fed synchronous machines." https://www.epfl.ch/labs/pel/wp-content/uploads/2021/05/2021.05.11_IEEE_Webinar_Direct-MMC-Control_export.pdf [Accessed on 06.07.2021].

[5] H. Schlunegger and A. Thöni, "100 MW full-size converter in the Grimsel 2 pumped-storage plant," *Innsbruck, Hydro*, 2013.

[6] A. Lesnicar and R. Marquardt, "An innovative modular multilevel converter topology suitable for a wide power range," in *2003 IEEE Bologna Power Tech Conference Proceedings,*, IEEE, vol. 3, 2003, 6–pp.

[7] M. Glinka and R. Marquardt, "A new ac/ac-multilevel converter family applied to a single-phase converter," in *The Fifth International Conference on Power Electronics and Drive Systems, 2003. PEDS 2003.*, IEEE, vol. 1, 2003, pp. 16–23.

[8] M. Vasiladiotis, R. Baumann, C. Häderli, and J. Steinke, "Igct-based direct ac/ac modular multilevel converters for pumped hydro storage plants," in *2018 IEEE Energy Conversion Congress and Exposition (ECCE)*, 2018, pp. 4837–4844.

[9] A. Zama, S. A. Mansour, D. Frey, A. Benchaib, S. Bacha, and B. Luscan, "A comparative assessment of different balancing control algorithms for modular multilevel converter (mmc)," in *2016 18th European Conference on Power Electronics and Applications (EPE'16 ECCE Europe)*, IEEE, 2016, pp. 1–10.

[10] H. A. Pereira, A. F. Cupertino, L. S. Xavier, A. Sangwongwanich, L. Mathe, M. Bongiorno, and R. Teodorescu, "Capacitor voltage balance performance comparison of mmc-statcom using nlc and ps-pwm strategies during negative sequence current injection," in *2016 18th European Conference on Power Electronics and Applications (EPE'16 ECCE Europe)*, IEEE, 2016, pp. 1–9.

[11] L. Mathe, "Performance comparison of the modulators with balancing capability used in mmc applications," in *2017 IEEE 26th International Symposium on Industrial Electronics (ISIE)*, IEEE, 2017, pp. 815–820.

[12] S. Milovanović and D. Dujić, "Comprehensive comparison of modular multilevel converter internal energy balancing methods," *IEEE Transactions on Power Electronics*, vol. 36, no. 8, pp. 8962–8977, 2021.

[13] F. Kammerer, J. Kolb, and M. Braun, "A novel cascaded vector control scheme for the modular multilevel matrix converter," in *IECON 2011-37th Annual Conference of the IEEE Industrial Electronics Society*, IEEE, 2011, pp. 1097–1102.

[14] F. Kammerer, M. Gommeringer, J. Kolb, and M. Braun, "Energy balancing of the modular multilevel matrix converter based on a new transformed arm power analysis," in *2014 16th European Conference on Power Electronics and Applications*, IEEE, 2014, pp. 1–10.

[15] F. Kammerer, J. Kolb, and M. Braun, "Fully decoupled current control and energy balancing of the modular multilevel matrix converter," in *2012 15th International Power Electronics and Motion Control Conference (EPE/PEMC)*, IEEE, 2012, LS2a–3.

[16] F. Kammerer, "Systemanalyse und regelung des modularen multilevel matrix umrichters als antriebsumrichter," 2016.

[17] A. J. Korn, M. Winkelnkemper, P. Steimer, and J. W. Kolar, "Capacitor voltage balancing in modular multilevel converters," in *6th IET International Conference on Power Electronics, Machines and Drives (PEMD 2012)*, 2012, pp. 1–5.

[18] M. Utvić and D. Dujić, "Generalized theory on direct arm energy control in modular multilevel converters," *CPSS Transactions on Power Electronics and Applications*, vol. 5, no. 4, pp. 388–399, 2020.

[19] P. Bontemps, S. Milovanovic, and D. Dujic, "Distributed real-time model of the m3c for hil systems using small-scale simulators," *IEEE Open Journal of Power Electronics*, vol. 2, pp. 603–613, 2021.

[20] J. Kucka, D. Karwatzki, and A. Mertens, "Ac/ac modular multilevel converters in wind energy applications: Design considerations," in *2016 18th European Conference on Power Electronics and Applications (EPE'16 ECCE Europe)*, 2016, pp. 1–10.

[21] P. Bontemps and D. Dujic, "Flexible operation of variable speed direct-mmc in hydropower applications," in *PCIM Europe 2022; International Exhibition and Conference for Power Electronics, Intelligent Motion, Renewable Energy and Energy Management*, IEEE, 2022.

[22] G. Strang and K. Borre, *Linear algebra, geodesy, and GPS*. Siam, 1997.

[23] E.ON Netz GmbH and Verband Der Netzbetreiber Vnd, *Transmissioncode 2007. network and system rules of the german transmission system operators*, https://www.vde.com/resource/blob/937766/bfe325518ace878935966b6efbc493e4/transmissioncode-2007--network-and-system-rules-of-the-german-transmission-system-operators-data.pdf [Accessed on 24.01.2022].